Nuclear Instruments and Methods in Physics Research B 406 (2017) 104–107

Contents lists available at ScienceDirect

Nuclear Instruments and Methods in Physics Research B

journal homepage: www.elsevier.com/locate/nimb

Thick multi-layers analysis using high energy PIXE

A. Subercaze [a,*], A. Guertin [a], F. Haddad [a,b], C. Koumeir [a,b], V. Métivier [a], N. Servagent [a]

[a] Laboratoire SUBATECH, Ecole des mines de Nantes, Université de Nantes, CNRS/IN2P3, 4 Rue Alfred Kastler, 44307 Nantes cedex 3, France
[b] GIP ARRONAX, 1 rue Aronnax, 44817 Saint-Herblain cedex, France

ARTICLE INFO

Article history:
Received 4 August 2016
Received in revised form 2 December 2016
Accepted 7 February 2017
Available online 20 February 2017

Keywords:
Ion beam analysis
High energy PIXE
Multi-layers

ABSTRACT

A method for multi-layer analysis using high energy PIXE is described. It is based on the variation of the $\frac{K_\alpha}{K_\beta}$ ratio as a function of the detection angle. Experiments have been carried out at the ARRONAX cyclotron using 70 MeV protons in order to validate this method. The thicknesses and the sequences of simple multi-layers targets and more complex targets with hidden layers have been determined using this method.

1. Introduction

High energy PIXE (HEPIXE), a technique using protons with energies higher than 10 MeV, has already been used to investigate piece of art and especially paintings [1–3]. High energy PIXE is a well-suited method for thick multi-layer analysis due to the large range of high energy protons. Using high energy particles beam allows to perform analysis in air and thus reduce the constraint on the sample preparation. The low energy loss of the high energy beam combined with a smooth variation of the K X-ray production cross sections in this energy range [4] induce a low variation of this cross section during the experiments. The data analysis is therefore simplified. So far, HEPIXE has been able to determine the thicknesses and the sequences of the layers [5] using $\frac{K_\alpha}{K_\beta}$ (or $\frac{K_\alpha}{L_\alpha}$, $\frac{L_\alpha}{L_\beta}$) ratio, but hypothesis on the sample composition is required. We have already developed a method to determine the thicknesses and the sequences of a simple ideal case [6]. Those ideal targets were composed of layers of pure material foils with no repetition of an element and without hidden layers. However, in real applications of multi-layer analysis (such as paintings or coins) there might be some layers composed of light elements, located at the surface or in the bulk that cannot be detected (hidden layers). Therefore, the method presented in [6] cannot be applied. In this work, we present a method to determine the thicknesses and the sequences of multi-layer targets with hidden layers.

2. Analysis method

Some observables sensitive to the thickness and the sequence of layers are required. For that purpose, we study the influence of the detection angle, (the angle between the sample and the detector), on the $\frac{K_\alpha}{K_\beta}$ ratio. The number of detected K_α X-rays is given by the equation:

$$N_{K_\alpha} = N_p \cdot \epsilon_\alpha \cdot \frac{1}{\mu'_\alpha} \cdot \frac{\Omega}{4.\pi} \cdot C \cdot b_\alpha \cdot \sigma \cdot (1 - e^{-\mu'_\alpha \cdot d'}) \prod_{i=0}^{n} e^{(-\mu^i_\alpha \cdot d^i)}, \quad (1)$$

where μ'_α and μ^i_α, are the attenuation coefficient [7] of the emitting layer and the layers, respectively, d' and d^i the X-ray path in the emitting layer and the layer i, respectively, which are a function of the detection angle θ. ϵ is the detector efficiency, b the line intensity faction [8], C the concentration of the emitting celement, Ω the detector solid angle, σ the cross section of the considered X-ray emission, N_p the number of protons crossing the target and n the number of layers placed ahead of the emitting one. In this equation, σ is considered as a constant due to its low variation (when using high energy beams). The $\frac{K_\alpha}{K_\beta}$ ratio, R, is given by the equation

$$R = \frac{N_{K_\alpha}}{N_{K_\beta}} = \frac{\mu_\beta}{\mu_\alpha} \cdot \frac{\epsilon_\alpha}{\epsilon_\beta} \cdot \frac{b_\alpha}{b_\beta} \cdot \frac{(1 - e^{(-\mu'_\alpha \cdot d')})}{(1 - e^{(-\mu'_\beta \cdot d')})} \cdot \prod_{i=0}^{n} \frac{e^{(-\mu^i_\alpha \cdot d^i)}}{e^{(-\mu^i_\beta \cdot d^i)}}. \quad (2)$$

Fig. 1 (a) shows both the experimental and the modelised variation of the $\frac{K_\alpha}{K_\beta}$ ratio in a single layer of titanium. The $\frac{K_\alpha}{K_\beta}$ ratio slightly varies in the layer itself meaning that it is barely sensitive to self attenuation. The variation of the self attenuation as a function of the detection angle is below the experimental errors, expected to

* Corresponding author.
E-mail address: subercaz@subatech.in2p3.fr (A. Subercaze).

http://dx.doi.org/10.1016/j.nimb.2017.02.014
0168-583X/

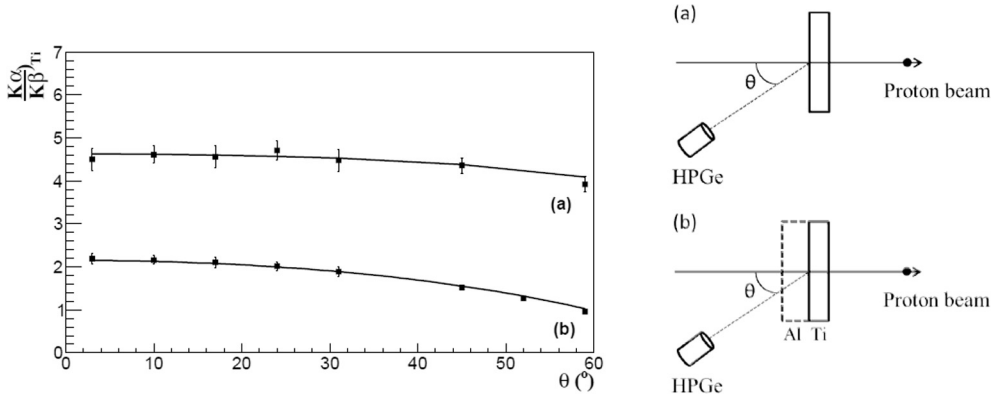

Fig. 1. Evolution of $\frac{K_\alpha}{K_\beta}$ ratio as a function of the detection angle using 68 MeV proton beam: (a) for a single layer of 10 μm of titanium, (b) for a layer of 50 μm of aluminium placed ahead of the emitting one (10 μm of titanium). The schemas represent those two experimental configurations. Dots are the experimental data and the lines correspond to the values calculated using Eq. (2).

be around 5%. Thus we consider the ratio $\frac{K_\alpha}{K_\beta}$ as a constant. Fig. 1 (b) shows also the variation of the $\frac{K_\alpha}{K_\beta}$ ratio of the same layer of titanium with a aluminium layer placed ahead. In this case, the ratio is dependent on a layer ahead of the emitting one. The ratio $\frac{K_\alpha}{K_\beta}$ contains the information about the amount of material in front of the considered layer and can be used to obtain the sequences and the thicknesses of a multi-layer target.

The relative variation of the $\frac{K_\alpha}{K_\beta}$ ratio as a function of the detection angle is given by:

$$\frac{\Delta R}{R} = \frac{R(\theta_1) - R(\theta_2)}{R(\theta_1)} = \frac{e^{\left(\frac{\Delta\mu\cdot d}{\cos(\theta_1)}\right)} - e^{\left(\frac{\Delta\mu\cdot d}{\cos(\theta_2)}\right)}}{e^{\left(\frac{\Delta\mu\cdot d}{\cos(\theta_1)}\right)}}, \tag{3}$$

where $\Delta\mu = \mu_{K_\beta} - \mu_{K_\alpha}$. With some algebra we can extract

$$\Delta\mu\cdot d = \frac{1}{\frac{1}{\cos(\theta_2)} - \frac{1}{\cos(\theta_1)}} \cdot \ln\left(\frac{1}{1-\frac{\Delta R}{R}}\right). \tag{4}$$

$\Delta\mu$.d contains the density, the chemical composition and the thickness of the effective layer between the emitting layer and the detector (the effective layer has the same effect on the X-ray attenuation than the sum of the real layers). Table 1 contains the values of $\Delta\mu\cdot d$ determined using Eq. 4 for the titanium layer in the configuration (b) of the Fig. 1. We only use the combinations of θ inducing the larger variation of R. Results show that $\Delta\mu\cdot d$ is independent of the choice of θ_1 and θ_2. Errors on $\Delta\mu\cdot d$ are mainly due to the error on $\frac{\Delta R}{R}$ and so to the error on the number of detected X-rays.

This term, $\Delta\mu\cdot d$, is also function of the X-ray energy thus implying that Eq. (4) cannot be used in this form to determine the sequences. Lets take into account the energy dependency of the photoelectric mass attenuation coefficient [9]

$$\frac{\mu}{\rho} = p\cdot\frac{1}{E^{\frac{7}{2}}}\cdot Z^5\cdot\frac{N_A}{A}, \tag{5}$$

Table 1
The values of $\Delta\mu\cdot d$ calculated using Eq. (4) for the titanium layer in the experimental configuration (b) in Fig. 1.

θ_1 (°)	θ_2 (°)	$\Delta\mu\cdot d$ (titanium)
45	3	−0.886 ± 0.058
45	10	−0.876 ± 0.055
45	17	−0.891 ± 0.054
45	24	−0.930 ± 0.056
45	31	−0.916 ± 0.056

where E is the energy of the considered X-ray, N_A is the Avogadro constant, Z the atomic number, p a constant and A the mass number. Now we can calculate a new parameter $(\Delta\mu\cdot d)'$ given by the Eq. (4)

$$(\Delta\mu\cdot d)' = \frac{1}{\frac{1}{(E_{K_\beta})^{\frac{7}{2}}} - \frac{1}{(E_{K_\alpha})^{\frac{7}{2}}}} \frac{1}{\frac{1}{\cos(\theta_2)} - \frac{1}{\cos(\theta_1)}} \cdot \ln\left(\frac{1}{1-\frac{\Delta R}{R}}\right), \tag{6}$$

where $(\Delta\mu\cdot d)'$ is also equal to $\rho\cdot d\cdot Z^5\cdot b\cdot\frac{N_a}{A}$. $(\Delta\mu\cdot d)'$ is a function of the properties of the effective layer between the detector and the considered layer. The smallest value of $(\Delta\mu\cdot d)'$ represents the lowest quantity of matter crossed by the X-rays. The comparison between the $(\Delta\mu\cdot d)'$ values of each detected element allows to determine the sequences.

Using Eq. (4) and (5), we can calculate the attenuation of K_α X-rays (or K_β) M_{K_α}

$$M_{K_\alpha} = \prod_{i=0}^{n} e^{(-\mu_\alpha^i\cdot d^i)} = e^{-\Delta\mu\cdot d\cdot\left(\frac{\frac{1}{(E_{K_\alpha})^{7/2}}}{\frac{1}{(E_{K_\beta})^{7/2}} - \frac{1}{(E_{K_\alpha})^{7/2}}}\right)}. \tag{7}$$

We can therefore correct the attenuation of the detected number of K_α X-rays, $N_{K_\alpha}^{layer}$, by using Eq. (7). The thickness of each layer is given by the comparison between the Eq. 1 for the layers and for the standard samples (irradiated in the same condition)

$$e_{layer} = -\frac{1}{\mu'_\alpha}\cdot ln\left(1 - \frac{N_{K_\alpha}^{layer}}{N_{K_\alpha}^{standard}\cdot M_{K_\alpha}}\right). \tag{8}$$

The errors on the thicknesses are calculated using the propagation error formula [10] and the associated errors of $\Delta\mu\cdot d, N_{K_\alpha}^{layer}$ and $N_{K_\alpha}^{standard}$.

3. Experimental set-up

PIXE experiments were carried out at ARRONAX cyclotron [11] using 68 MeV protons. The experimental set-up is described in more details in [6]. The X-rays are detected by a High Purity Germanium (HPGe) detector. The distance between the sample and the detector is 25 cm. The sample holder can be tilted with respect to the incident beam in order to change the angle between the sample and the detector. We use a thin foil of copper (2 μm) in order to monitor the number of particles crossing the target. This monitor foil is placed ahead of every target and is in contact with the samples.

4. Investigated targets

The analysis method described above is used on both ideal targets, composed of pure material foils with no repetition of the same elements, similar to the multi-layers targets studied in [6] and on more complex cases, where some layers are hidden. The targets used in this work are listed in Table 2.

In this particular set-up aluminium is used to simulate hidden layers.

Standard targets for each detected element have also been irradiated in the same experimental condition.

5. Results and discussion

Fig. 2 shows spectra of the studied targets. In both targets, X-rays from the monitor foil of copper are detected. We can notice that the X-rays from aluminium (1.486 keV) are not visible in the spectrum of the second target due to the high attenuation of low energy X-rays emitted by aluminium.

Using Eqs. (6) and (8), we have determined the $(\Delta\mu \cdot d)'$ values and the thicknesses of the foils for each target (Table 3). The experimental errors on the $(\Delta\mu \cdot d)'$ values and on the calculated thicknesses are only due to the statistical errors on the detected K-lines number. The calculated thicknesses and the sequences for the first target are in a good agreement with the calibrated thicknesses and the positions of each layers. The value of $(\Delta\mu \cdot d)'$ for titanium is not as close to zero as it should be (because it's the first layer). This is due to the monitor foil.

For the more complex target, the calculated thicknesses of the two elements detected are in a good agreement with the calibrated ones (Table 3) even though the two aluminium layers aren't detected. The high values for $(\Delta\mu \cdot d)'$ reveal the presence of some hidden layers in the sample. The values of $(\Delta\mu \cdot d)'$ for the titanium and the silver are far from the value of the simple target, which means there is one or more layer in front of the titanium and between the titanium and the silver.

Table 2
Composition of the investigated targets. The position gives the location of the layer inside the target. Position 1 is closest to the surface and 3 (or 4) is the last position.

Target 1		Target 2	
Element	Position	Element	Position
Titanium	1	Aluminium	1
Silver	2	Titanium	2
Gold	3	Aluminium	3
–	–	Silver	4

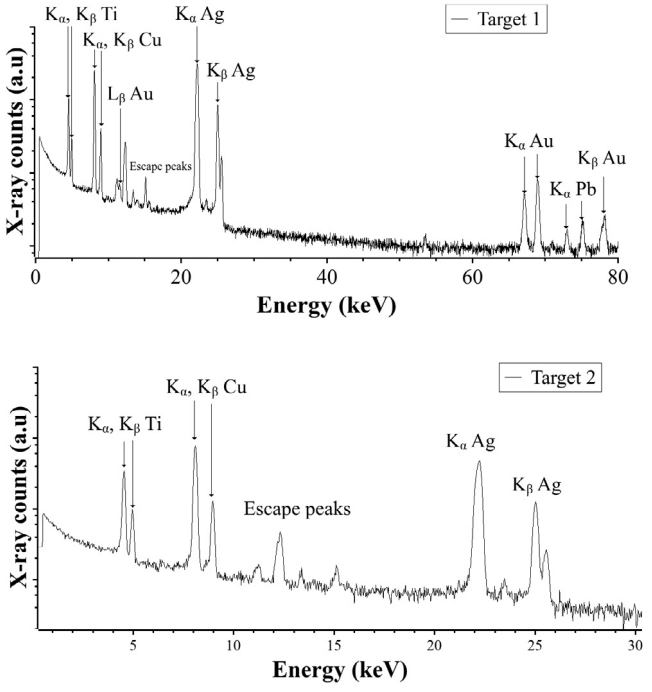

Fig. 2. Spectra of the investigated targets obtained using 68 MeV proton beam at the detection angle of 3°. First spectrum: ideal sample consisting of thick silver and gold layers. Second spectrum: sample consisting of two thick aluminium, titanium and silver layer. The X-ray from copper visible in those spectra are due to the presence of the monitor foil.

Table 3
Results of the multi-layers analysis using detection angles of 3° and 45°.

Element	$(\Delta\mu \cdot d)'$	Calculated thickness (μm)	Calibrated thickness (μm)
Target 1			
Titanium	92 ± 6	10.40 ± 0.62	10.03 ± 0.02
Silver	860 ± 40	25.82 ± 1.29	24.87 ± 0.04
Gold	12,200 ± 600	9.11 ± 0.59	10.74 ± 0.02
Target 2			
Titanium	664 ± 62	9.25 ± 0.93	10.06 ± 0.02
Silver	4168 ± 348	10.33 ± 0.21	10.32 ± 0.02

6. Conclusions

High energy PIXE provides high indepth analysis thanks to the range of high energy beam, the slow variation of the ionization cross section and the low energy loss of 68 MeV protons beam. The self attenuation in the emitting layer has little impact on the variation of $\frac{K_\alpha}{K_\beta}$ as a function of the detection angle but this ratio is sensitive to the layers located above and contains information about those layers. Those properties allow us to use this ratio to determine the thicknesses and the sequences of the layers in a target which contains undetected layers at the surface and/or in the bulk. Furthermore, we dont't have to make any hypothesis on the composition of the undetected layers in order to perform the analysis. Further studies are ongoing to determine the minimum and maximum thicknesses achievable with this method, which depends on the investigated element, the detection limit and the position of the layer in the target.

Acknowledgments

The ARRONAX cyclotron is a project promoted by the Regional Council of Pays de la Loire financed by local authorities, the French government and the European Union. This work has been, in part, supported by a grant from the French National Agency for Research called 'Investissements d'Avenir', Equipex Arronax-Plus no ANR-11-EQPX-0004 and Labex no ANR-11-EQPX-0018–01.

References

[1] A. Denker, K. Maier, Investigation of objects d'art by PIXE with 68 MeV protons, Nucl. Instr. Meth. Phys. Res. B 161–163 (2000) 704–708.
[2] A. Denker, M. Blaich, PIXE analysis of Middle age objects using 68 MeV protons, Nucl. Instr. Meth. Phys. Res. B 189 (2002) 315–319.
[3] T. Dupuis, Preliminary experiments: high-energy alpha PIXE in archaeometry, Nucl. Instr. Meth. Phys. Res. B 268 (2010) 1911–1915.
[4] S.J. Cippola, ISICS2008: An expanded version of ISICS for calculating K-, L-, and M-shell cross sections from PWBA and ECPSSR theory, Comput. Phys. Commun. 180 (2009) 1716–1717.
[5] A. Denker, J. Optiz-Coutureau, Paintings-high-energy protons detect pigments and paint-layers, Nucl. Instr. Meth. Phys. Res. B 213 (2004) 677–682.
[6] D. Ragheb, al, Development of a PIXE method at high energy with the ARRONAX cyclotron, J. Radioanal. Nucl. Chem. 301 (2014) 895–901.

[7] National Institute of Standards and Technology (Jun. 2016). URL http://physics.nist.gov/PhysRefData/Xcom/html/xcom1.html.
[8] J. Scofield, Exchange corrections of K X-ray emission rates, Phys. Rev. A 9 (1974) 1041–1049.
[9] W. Heitler, The Quantum Theory of Radiation, Oxford Univ Press, 207–208.
[10] G.F. Knoll, Radiation Detection and Measurement, fourth ed., Wiley, 2010.
[11] F. Haddad, al, Arronax a high-energy and high-intensity cyclotron for nuclear medicine, Eur. J. Nucl. Med. Mol. Imag. 35 (2008) 1377–1387.